PCCP

PAPER

View Article Online
View Journal | View Issue

Dissociation rates of H_2 on a Ni(100) surface: the role of the physisorbed state

Cite this: *Phys. Chem. Chem. Phys.*, 2014, **16**, 13318

Wenji Wang*[a] and Yi Zhao[b]

The dissociation and recombination rates of physisorbed H_2, and the total dissociation rate of gas phase H_2 on the rigid Ni(100) surface, as well as the corresponding kinetic isotope effects, are calculated by using the quantum instanton method, together with path integral Monte Carlo and adaptive umbrella sampling techniques. Both the dissociation and recombination rates of physisorbed H_2 are dramatically enhanced by the quantum motions of H_2 at low temperatures, for instance, the quantum rates are 43 and 7.5 times larger than the classical ones at 200 K, respectively. For the dissociation of gas phase H_2, at high temperatures, the H_2 can fly over the physisorbed state and dissociate directly, however, at low temperatures, the H_2 is first physisorbed and then dissociates under steady state approximation. The total dissociation rate of gas phase H_2 can be expressed as a combination of the direct and steady state dissociation rates. It has the form of an inverted bell with a minimum value at about 400 K, and detailed analysis shows that the dissociation of gas phase H_2 is dominated by a steady state process below 400 K, however, both the steady state and direct processes are important above 400 K. The calculated kinetic isotope effects reveal that H_2 always has larger rates than D_2 no matter which dissociative process they undergo.

Received 19th April 2014,
Accepted 15th May 2014

DOI: 10.1039/c4cp01705f

www.rsc.org/pccp

1 Introduction

The dissociative adsorption of hydrogen on nickel surfaces is one of the most extensively investigated subjects.[1–4] This is not only because the understanding of the dynamic of this process is important for elucidating the microscopic mechanisms of metal–adsorbate reactions, but also because nickel catalysts are commonly used in many industrial processes like hydrogenation, methanation and steam reforming of hydrocarbons.

The dissociation and recombination of H_2 on a Ni(100) surface have been investigated both experimentally and theoretically. On the experimental side, the techniques of molecular beam,[5] high-resolution electron energy loss spectra[6] and static secondary ion mass spectroscopy[7,8] have been used, and a great deal of information is available.[9–12] On the theoretical side, several kinds of potential energy surfaces (PESs)[13–18] have been constructed. Based on PESs, the classical,[14,19] mixed quantum-classical[20,21] and rather complex quantum mechanical[22–24] simulations have been used to reveal the microscopic mechanisms of these kinds of reactions,[25–45] moreover, the effect of the lattice motions has also been incorporated in several simulations.[46–53] In spite of the great progress that has already been made in our understanding of the features of the title reaction, some controversies still exist. For instance, the role of the physisorbed state in the dissociation process has not been elucidated.

Experimentally, Hamza and Madix[5] reported a direct mechanism of dissociation for H_2 and D_2 on a Ni(100) surface with nearly mono-energetic beams of hydrogen and deuterium. However, Rendulic *et al.*[10] showed that there exists a mixture of activated and non-activated adsorption paths, and at low temperatures a small amount of hydrogen adsorbs through a precursor, by performing angle resolved measurements of the sticking coefficient for H_2 on Ni(100). Zhu *et al.*[11] also reported the evidence for the coexistence of direct and precursor dynamics in the dissociative chemisorption of H_2 on Ni(100), they found that a molecular precursor mediates dissociative adsorption at low temperatures, and a direct dissociation channel dominates the process for $T > 200$ K.

Theoretically, Gross *et al.*[54,55] attributed the increase of the sticking probability with decreasing kinetic energy at low kinetic energies to a purely dynamically steering effect for the H_2–Pd(100) system, in which neither potential barrier nor molecular adsorption well exists. For the H_2–Ni(100) system, Kresse[19] demonstrated that the high sticking coefficient is related to a combination of steering at low energies and direct activated dissociation at high beam energies. Although no physisorbed molecular hydrogen has been found on clean Ni(100),[56] Andersson and co-workers reported that molecular hydrogen is held on Ni(100) at 150 K in the presence of coadsorbed CO,[57] so it should be reasonable to assume that the physisorbed state exists for the H_2/Ni(100) dissociative process (indeed, the

[a] College of Science, Northwest A&F University, Yangling, 712100, Shaanxi Province, P. R. China. E-mail: wjwang@nwsuaf.edu.cn

[b] State Key Laboratory for Physical Chemistry of Solid Surfaces and Fujian Provincial Key Lab of Theoretical and Computational Chemistry, College of Chemistry and Chemical Engineering, Xiamen University, Xiamen, 361005, P. R. China

physisorbed state exists in many systems, such as H_2–Cu(111)[44] and H_2–Pd(110)[58]), and consider it as a model system, in this case, this dissociative process may be affected by both the steering effect and the physisorbed state. In the present work, we focus on the effects of the physisorbed state.

Lee and DePristo[15] constructed a potential energy surface for the dissociative chemisorption of H_2 on Ni(100), which is based upon a delocalized effective medium form plus empirical two-body terms, on this PES a potential well exists which corresponds to a physisorbed state. Based on a modified version of Lee and DePristo's PES, Truong *et al.*[26] applied canonical variational transition state theory to examine the dynamics of the dissociative chemisorption of H_2 and D_2 on Ni(100). In their calculations, they have applied the steady state approximation which assumes that the concentration of the physisorbed H_2 molecule remains constant during the time of exposure. However, several years later, Chakravarty and Metiu[59] used the correlation function theory, which provides equations expressing the rate constants in terms of flux-position correlation functions, to distinguish the direct and precursor dynamics through the mean time spent by the H_2 molecule in the physisorption well. They found that the lifetime of physisorbed H_2 is extremely short at 300 K, so it is then justified in treating the dynamics as a direct dissociation and ignoring physisorption, but at 100 K physisorbed H_2 has a long lifetime and one is forced to consider a two-step dynamics: H_2 is first physisorbed and then dissociated. Though the work of Chakravarty and Metiu has provided reasonable results, it is classical and offering no prescription for intermediate temperatures.

For the present reaction, a remarkable kinetic isotope effect (KIE) has also been reported. Experimentally, Hamza and Madix[5] showed that the initial dissociative sticking probability for D_2 is lower than that of H_2, and reported that the barrier height is 1.2 kcal mol^{-1} for H_2 and 1.6 kcal mol^{-1} for D_2. Zhu *et al.*[11] reported that the average sticking coefficient of H_2 is higher than that of D_2 at 200 K. Theoretically, Mowrey[60] found that the D_2 needs at least 0.67 kcal mol^{-1} additional energy than the H_2 to pass over the top of the barrier. Truong *et al.*[26] calculated the H_2 and D_2 dissociation rate constants, the ratios are 6.6, 4.0, 3.0 and 2.3 at 200, 300, 500 and 800 K, respectively, they also found that the quantum mechanical tunneling enhances the kinetic isotope effect a lot.

In the present paper, we investigate the dissociation and recombination of H_2 on a rigid Ni(100) surface with two specific goals. One is to reveal the quantum effect and kinetic isotope effect during the reaction and examine how they affect rates. The other is to make a systematic analysis of the role of the physisorbed state in the dissociative process over a wide range of temperatures. The absence of lattice motion will limit the accuracy of the calculated rates, in our previous work,[53] we have demonstrated that the classical and quantum motions of the lattice enhance the physisorbed H_2 dissociation rates by 18% and 49% at 300 K, however, we will not consider it in the present work. To calculate the rates, we use the quantum instanton (QI) approach which is originally proposed by Miller *et al.*[61] for the calculations of reaction rates. The approximation of QI is similar to an earlier semiclassical TST[62] that became known as the instanton model,[63] but it has an advantage that the Boltzmann operator is treated fully quantum mechanically rather than within the semiclassical approximation. The QI method considers all tunneling paths and automatically gives each path its natural weight by the quantum Boltzmann factor and incorporates the quantum-fluctuation effect correctly. In addition, the QI method can be applied in Cartesian space with a full dimensional potential energy surface, taking into account the effects of the vibrational–rotational coupling and anharmonicity of the reaction system naturally. It has been successfully applied to gas phase reactions,[64–67] proton transfer,[68,69] surface diffusions,[70–72] torsional anharmonicity[73,74] and kinetic isotope effects.[75–78]

The remainder of this paper is as follows: The reaction mechanism is presented in Section 2. In Section 3, we first summarize the working expression of the QI theory, and then apply it to the title reaction. Section 4 describes the computational details. Section 5 gives the numerical results of rates and kinetic isotope effects. Section 6 is the concluding remarks.

2 Reaction mechanism

In this section, we present the mechanism of the H_2/Ni(100) reaction on a rigid surface, thus we neglect the motions of metal atoms. In the modified version[26] of Lee and DePristo's PES,[15] the classical potential energy barrier from the gas phase H_2 to two chemisorbed H atoms is -0.3 kcal mol^{-1}, which is much lower than the barrier (3.46 kcal mol^{-1}) reported by Kresse[19] with the density functional theory. This discrepancy is mainly caused by the fact that this modified PES involves a physisorbed state (-3.1 kcal mol^{-1}), and the classical potential energy barrier from this physisorbed state to chemisorbed state is 2.8 kcal mol^{-1}. The zero point energy corrected potential energies at the physisorbed and transition states are -1.4 and 0.6 kcal mol^{-1} respectively, relative to the overall zero of energy which is set at the infinite separation of H_2 from the surface, so the effective barrier to chemisorption from the physisorbed state is 2.0 kcal mol^{-1}. Since the potential well at the physisorbed state is deep, it is probably that the hydrogen molecules with low energies will be trapped in the physisorbed state, while that with high energies may pass over it directly.

At low temperatures, it is reasonable to assume that physisorbed H_2 is formed and equilibrated,[26] by applying the steady state approximation, the reaction can be modeled by the following set of reactions

$$H_2(g) + S \underset{k_{-1}}{\overset{k_1}{\rightleftharpoons}} H_2(a) - S, \quad (1)$$

$$H_2(a) - S \underset{k_{-2}}{\overset{k_2}{\rightleftharpoons}} 2H(a) - S. \quad (2)$$

Here, S represents the empty site on the Ni surface. k_1 is the rate constant (cm^3 site^{-1} s^{-1}) for the molecular adsorption of gas phase H_2 molecules; k_{-1} is the rate constant (s^{-1}) of the desorption of adsorbed H_2 molecules; k_2 is the rate constant (s^{-1}) of the dissociative chemisorption of adsorbed H_2 molecules; and k_{-2} is the recombination rate (s^{-1}) of H_2. The overall steady state rate constant k_{steady}(cm^3 site^{-1} s^{-1}) can be written as

$$k_{\text{steady}} = \frac{k_1 k_2}{k_{-1} + k_2}. \quad (3)$$

At high temperatures, the H_2 molecules have enough energies to pass over the physisorbed state, so the dissociation reaction should be direct,[59]

$$H_2(g) + S \overset{k_{direct}}{\rightleftharpoons} 2H(a) - S. \quad (4)$$

However, at intermediate temperatures, the physisorption mediated process and the direct process should coexist. The total rate constant k could be expressed using the following formula

$$k = k_{direct} \times f + k_{steady} \times (1 - f), \quad (5)$$

where f is the fraction of gas phase H_2 that has an energy greater than or equal to a certain value E_1, with which the gas phase H_2 can fly over the physisorbed state. The relation $E_{GS} \geq E_1$ can be further written as

$$E_{GS}(H_2) - E_{PS}^{G}(H_2) \geq V_{GS}(H_2) - V_{PS}(H_2), \quad (6)$$

with

$$E_{GS}(H_2) = E_{GS}^{tr}(H_2) + E_{GS}^{rot}(H_2) + E_{GS}^{vib}(H_2), \quad (7)$$

where E_{GS} denotes the summation of the translational (E_{GS}^{tr}), rotational (E_{GS}^{rot}) and vibrational (E_{GS}^{vib}) energies of H_2 in the gas phase. E_{PS}^{G} stands for the minimum vibrational energy that the physisorbed H_2 must hold, since all the rotational and translational modes of physisorbed H_2 are restricted, we treat them as vibrational modes, and the superscript 'G' stands for all six vibrational modes of physisorbed H_2 treated as being in the ground state when calculating the minimum vibrational energy. V_{GS} and V_{PS} represent the classical potential energies of H_2 in the gas phase and physisorbed state. Overall, eqn (6) and (7) mean that part of the energy of gas phase H_2 will convert to the minimum vibrational energy of physisorbed H_2, and the rest can be used to overcome the potential well in the physisorbed state.

According to statistical mechanics, the characteristic rotational and vibrational temperatures of gas phase H_2 are 88 and 5987 K, which mean that the rotational degrees of freedom are well excited and the vibrational mode of motion is frozen out in our tested temperature range of 160–800 K. So the vibrational energy of gas phase H_2 is equal to the ground state energy ($\hbar\omega/2$) which can be obtained by vibrational frequency (ω), and the rotational energy (k_BT per molecule) of gas phase H_2 can be obtained from the equipartition theorem. By substituting the vibrational (using the vibrational frequencies of both gas phase and physisorbed H_2), rotational and classical potential energies into eqn (6), we get

$$E_{GS}^{tr}(H_2) \geq 4.75(\text{kcal mol}^{-1}) - k_BT. \quad (8)$$

Now, we can use the Maxwell–Boltzmann distribution, the fraction of hydrogen molecules with translational energy equal to or in excess of E_2 ($E_2 = 4.75(\text{kcal mol}^{-1}) - k_BT$) can be expressed as

$$f_{MB}(E_2) = \frac{2}{\sqrt{\pi}} a e^{-a^2} + \text{erfc}(a), \quad (9)$$

where $a = (E_2/k_BT)^{1/2}$ and erfc(a) is the co-error function.

Finally, the total rate constant k in eqn (5) could be expressed as follows

$$k = k_{direct} \times f_{MB}(E_2) + k_{steady} \times (1 - f_{MB}(E_2)). \quad (10)$$

3 Rate theory

3.1 Summary of the quantum instanton theory

In this section, we summarize the work formulas for the QI approximation. The detailed derivation can be found in ref. 61, 64 and 65. The QI model proposes the following thermal rate constant

$$k_{QI}Q_r = \frac{\sqrt{\pi}\hbar}{2} \frac{C_{ff}(0)}{\Delta H(\beta)}. \quad (11)$$

Here, Q_r is the reactant partition function per unit volume. $C_{ff}(0)$ is the zero time value of the flux–flux correlation function

$$C_{ff}(t) = \text{tr}[e^{-\beta\hat{H}/2}\hat{F}_a e^{-\beta\hat{H}/2} e^{i\hat{H}t/\hbar}\hat{F}_b e^{-i\hat{H}t/\hbar}], \quad (12)$$

where β is the inverse temperature ($1/(k_BT)$), $\hat{H}$ is the Hamiltonian operator of the reaction system, and $\hat{F}_a$ and $\hat{F}_b$ are the flux operators, given by

$$\hat{F}_\gamma = \frac{i}{\hbar}[\hat{H}, h(s_\gamma(\hat{\mathbf{r}}))], \quad (13)$$

with γ = a, b. In eqn (13), h is the Heaviside function, r represents the Cartesian coordinates of the reaction system, and $s_a(r)$ and $s_b(r)$ define two separate dividing surfaces *via* the equations $s_a(r) = 0$ and $s_b(r) = 0$, both $s_a(r)$ and $s_b(r)$ being positive (negative) on the product (reactant) side of the dividing surfaces.

ΔH in eqn (11) is a specific type of energy variance, given by

$$\Delta H(\beta) = \hbar\sqrt{\frac{-\ddot{C}_{dd}(0)}{2C_{dd}(0)}}. \quad (14)$$

In order to get the correct free particle (high temperature) limit (that would be 25% too large otherwise), an ad hoc term is added to $\Delta H(\beta)$, $\Delta H_{mod}(\beta) = \Delta H(\beta) + (\sqrt{\pi} - \sqrt{2})/\beta$, which has very little effect in the low temperature regime. $C_{dd}(0)$ and $\ddot{C}_{dd}(0)$ are zero time value and its second time derivative, respectively, of the "delta–delta" correlation function

$$C_{dd}(t) = \text{tr}[e^{-\beta\hat{H}/2}\Delta(s_a(\hat{\mathbf{r}}))e^{-\beta\hat{H}/2} e^{i\hat{H}t/\hbar}\Delta(s_b(\hat{\mathbf{r}}))e^{-i\hat{H}t/\hbar}], \quad (15)$$

where the generalized delta-function operator is

$$\Delta(s_\gamma(\hat{\mathbf{r}})) = \delta(s_\gamma(\hat{\mathbf{r}}))\sqrt{\sum_{i=1}^{N}\frac{1}{m_i}(\nabla_i s_\gamma(\hat{\mathbf{r}}))^2} \quad (\gamma = a,\ b). \quad (16)$$

Here, N is the total number of atoms, $\nabla_i = \partial/\partial r_i$, r_i denotes the Cartesian coordinates of the ith atom and m_i is its atomic mass.

The dividing surfaces are determined by the stationary condition

$$\frac{\partial}{\partial c_k} C_{dd}(0; \{c_k\}) = 0, \quad (17)$$

where $\{c_k\}$ is a collection of parameters that is involved in the location of the dividing surfaces. This condition originates from the SC instanton model, and the resulting dividing surfaces correspond qualitatively to the turning points of the periodic orbit that runs on an upside down PES in imaginary time.

3.2 Path integral evaluation of the quantum instanton rate

Since all the relevant quantities in the QI expression (eqn (11)) involve only the quantum Boltzmann operator, they can be readily evaluated using the imaginary time Path Integral Monte Carlo (PIMC)[79] method. In realistic calculations, we rewrite eqn (11) as the product of several ratios

$$k_{\mathrm{QI}} = \frac{\sqrt{\pi}\hbar}{2}\frac{C_{\mathrm{dd}}(0)}{Q_{\mathrm{r}}}\frac{C_{\mathrm{ff}}(0)}{C_{\mathrm{dd}}(0)}\frac{1}{\Delta H(\beta)}. \tag{18}$$

The terms of $C_{\mathrm{ff}}(0)/C_{\mathrm{dd}}(0)$ and ΔH are directly calculated as a constrained average over the same ensemble of paths[64,65]

$$C_{\mathrm{ff}}(0)/C_{\mathrm{dd}}(0) = \langle f_{\mathrm{v}}\rangle_{\ddagger}, \tag{19}$$

$$\Delta H^2 = \tfrac{1}{2}\langle F^2 + G\rangle_{\ddagger}, \tag{20}$$

where

$$f_{\mathrm{v}} = \left(\frac{iP}{2\hbar\beta}\right)^2 \frac{\sum_{i=1}^{N}\nabla_i s_{\mathrm{a}}\left(r^{(0)}\right)\cdot\left(r_i^{(1)} - r_i^{(P-1)}\right)}{\sqrt{\sum_{i=1}^{N} m_i^{-1}\left(\nabla_i s_{\mathrm{a}}\left(r^{(0)}\right)\right)^2}} \times \frac{\sum_{i=1}^{N}\nabla_i s_{\mathrm{b}}\left(r^{(P/2)}\right)\cdot\left(r_i^{(P/2+1)} - r_i^{(P/2-1)}\right)}{\sqrt{\sum_{i=1}^{N} m_i^{-1}\left(\nabla_i s_{\mathrm{b}}\left(r^{(P/2)}\right)\right)^2}}, \tag{21}$$

and

$$F = -\frac{P}{\hbar^2\beta^2}\left\{\sum_{s=1}^{P/2} - \sum_{s=P/2+1}^{P}\right\}\sum_{i=1}^{N} m_i\left(r_i^{(s)} - r_i^{(s-1)}\right)^2 + \frac{2}{P}\left\{\sum_{s=1}^{P/2-1} - \sum_{s=P/2+1}^{P-1}\right\}V\left(r^{(s)}\right), \tag{22}$$

$$G = \frac{2fP}{\beta^2} - \frac{4P}{\hbar^2\beta^3}\sum_{s=1}^{P}\sum_{i=1}^{N} m_i\left(r_i^{(s)} - r_i^{(s-1)}\right)^2. \tag{23}$$

Here, P is the number of imaginary time slices, and m_i denotes the mass of the ith H atom. $r^{(s)}$ and $r_i^{(s)}$ represent the Cartesian coordinates for the sth time slice and for the sth time slice of the ith H atom, respectively. f is the degree of freedom for quantized H atoms. $\Delta\beta$ is defined by $\Delta\beta = \beta/P$.

The $\langle\cdots\rangle_{\ddagger}$ in eqn (19) represents the constrained path average

$$\langle\cdots\rangle_{\ddagger} = \frac{\int dr^{(1)}\int dr^{(2)}\cdots\int dr^{(P)}\Delta\left(s_{\mathrm{a}}\left(r^{(0)}\right)\right)\Delta\left(s_{\mathrm{b}}\left(r^{(P/2)}\right)\right)\exp[-\beta\Phi](\cdots)}{\int dr^{(1)}\int dr^{(2)}\cdots\int dr^{(P)}\Delta(s_{\mathrm{a}}(r^{(0)}))\Delta(s_{\mathrm{b}}(r^{(P/2)}))\exp[-\beta\Phi]}, \tag{24}$$

with

$$\Phi = \frac{P}{2\hbar^2\beta^2}\sum_{s=1}^{P}\sum_{i=1}^{N} m_i\left(r_i^{(s)} - r_i^{(s-1)}\right)^2 + \frac{1}{P}\sum_{s=1}^{P} V\left(r^{(s)}\right). \tag{25}$$

The evaluation of $C_{\mathrm{dd}}(0)/Q_{\mathrm{r}}$, however, meets a challenge because the $C_{\mathrm{dd}}(0)$ is the quantity associated with the transition state, while Q_{r} with the asymptotic reactant domain. First, we write it to be

$$C_{\mathrm{dd}}(0)/Q_{\mathrm{r}} = \frac{\mathrm{tr}\left[e^{-\beta\hat{H}/2}\Delta(s_{\mathrm{a}}(\hat{\mathbf{r}}))e^{-\beta\hat{H}/2}\Delta(s_{\mathrm{b}}(\hat{\mathbf{r}}))\right]}{\mathrm{tr}\left[e^{-\beta\hat{H}/2}\delta\left(s_{\mathrm{a}}^0(\hat{\mathbf{r}})\right)e^{-\beta\hat{H}/2}\delta\left(s_{\mathrm{b}}^0(\hat{\mathbf{r}})\right)\right]} \times \frac{\mathrm{tr}\left[e^{-\beta\hat{H}/2}\delta\left(s_{\mathrm{a}}^0(\hat{\mathbf{r}})\right)e^{-\beta\hat{H}/2}\delta\left(s_{\mathrm{b}}^0(\hat{\mathbf{r}})\right)\right]}{Q_{\mathrm{r}}}, \tag{26}$$

where s_{a}^0 and s_{b}^0 denote the reaction coordinates in the reactant region. Then, the first term on the right in eqn (26) can be solved by using eqn (16) and the adaptive umbrella sampling technique.[80] For the second one, it is evaluated directly when calculating the rate k_2 (Q_{r} is written as $\mathrm{tr}[e^{-\beta\hat{H}/2}h(s_{\mathrm{a}}^0(\hat{\mathbf{r}}))e^{-\beta\hat{H}/2}h(s_{\mathrm{b}}^0(\hat{\mathbf{r}}))]$, where $h(s_{\mathrm{a}}^0)$ and $h(s_{\mathrm{b}}^0)$ constrain the hydrogen molecule in the physisorbed state), and it is evaluated analytically when calculating the rate k_{direct} (see Appendix).

The free energy surface is defined by

$$F(s_{\mathrm{a}},s_{\mathrm{b}}) = -k_{\mathrm{B}}T\log[C_{\mathrm{dd}}(0;s_{\mathrm{a}},s_{\mathrm{b}})], \tag{27}$$

and the free energy profile along the reaction path is defined by

$$F(s) = -k_{\mathrm{B}}T\log[C_{\mathrm{dd}}(0;s,s)], \tag{28}$$

where $s = s_{\mathrm{a}} = s_{\mathrm{b}}$.

3.3 Application to the H_2/Ni(100) reaction

We now apply the QI method to the hydrogen molecule dissociation and recombination reactions on a Ni(100) surface. In the present calculations, the modified version[26] of Lee and DePristo's PES[15] is adopted, and all six degrees of freedom of H_2 are included. In this PES, both the physisorbed state and transition state have asymmetric orientations, this phenomenon is in conflict with the conventional idea that symmetric geometries are more favorable, such as H_2/Pd(100).[55] However, this PES should be reasonable, and choosing it allows us to compare our results to previous rate constant calculations.[26,59]

To calculate the rates, it is necessary to define a generalized reaction coordinate $s(r;\xi)$, where ξ is an adjustable parameter that shifts the location of the dividing surface (defined by $s(r;\xi) = 0$). The essential strategy for defining $s(r;\xi)$ is the same as that in the paper,[65] *i.e.*, $s(r;\xi)$ is defined by a linear interpolation

between two constituent reaction coordinates $s_0(r)$ and $s_1(r)$ through the parameter ξ,

$$s(r;\xi) = \xi s_1(r) + (1 - \xi)s_0(r). \quad (29)$$

For the dissociation process, $s_1^{\mathrm{dis}}(r)$ is a reaction coordinate whose dividing surface is designed to pass through the top of the classical potential barrier. It is noted that the position of potential barrier is determined by both the bond length of H_2 and the distance of the center of mass of H_2 above the surface. We thus define $s_1^{\mathrm{dis}}(r)$ as follows

$$\begin{aligned} s_1^{\mathrm{dis}}(r) &= \frac{Z_{\mathrm{TS}}(\mathrm{H}^1) + Z_{\mathrm{TS}}(\mathrm{H}^2)}{2} - \frac{Z(\mathrm{H}^1) + Z(\mathrm{H}^2)}{2} \\ &\quad - \left[R_{\mathrm{TS}}(\mathrm{H}^1 - \mathrm{H}^2) - R(\mathrm{H}^1 - \mathrm{H}^2)\right], \end{aligned} \quad (30)$$

where $Z(\mathrm{H}^1)$ and $Z(\mathrm{H}^2)$ are the coordinates of z-axis (vertical to Ni(100) surface) for the two hydrogen atoms (H^1 and H^2), respectively. R(X–Y) denotes the interatomic distance between atoms X and Y. The subscript TS denotes the values at the transition state geometry. $s_0^{\mathrm{dis}}(r)$ in eqn (29), on the other hand, describes a dividing surface that is located in the reactant region, which is given by

$$\begin{aligned} s_0^{\mathrm{dis}}(r) &= \frac{Z_R(\mathrm{H}^1) + Z_R(\mathrm{H}^2)}{2} - \frac{Z(\mathrm{H}^1) + Z(\mathrm{H}^2)}{2} \\ &\quad - \left[R_R(\mathrm{H}^1 - \mathrm{H}^2) - R(\mathrm{H}^1 - \mathrm{H}^2)\right], \end{aligned} \quad (31)$$

where the subscript R represents the values in the reactant region (it should be mentioned that the physisorbed state is regarded as the reactant when calculating the rate k_2, while for the rate k_{direct}, the gas phase state is the reactant).

Similarly, the reaction coordinates $s_1^{\mathrm{rec}}(r)$ and $s_0^{\mathrm{rec}}(r)$ for the recombination process are given by

$$s_1^{\mathrm{rec}}(r) = -s_1^{\mathrm{dis}}(r), \quad (32)$$

$$\begin{aligned} s_0^{\mathrm{rec}}(r) &= \frac{Z(\mathrm{H}^1) + Z(\mathrm{H}^2)}{2} - \frac{Z_P(\mathrm{H}^1) + Z_P(\mathrm{H}^2)}{2} \\ &\quad - \left[R(\mathrm{H}^1 - \mathrm{H}^2) - R_P(\mathrm{H}^1 - \mathrm{H}^2)\right], \end{aligned} \quad (33)$$

where the subscript P stands for the values at the product domain (the chemisorbed state where two separated hydrogen atoms are chemisorbed in two fourfold hollow sites).

The above definition makes the reaction coordinate only related to one parameter ξ with $s(r;0) = s_0(r)$ and $s(r;1) = s_1(r)$. As ξ changes from 0 to 1, the dividing surface moves smoothly from the reactant (product) domain to the transition state region.

$C_{\mathrm{dd}}(0)$ (in eqn (15)) now becomes a function of two parameters (ξ_a,ξ_b)[64,65]

$$C_{\mathrm{dd}}(0;\xi_a,\xi_b) = \mathrm{tr}[e^{-\beta\hat{H}/2}\Delta(s(\hat{\mathbf{r}},\xi_a))e^{-\beta\hat{H}/2}\Delta(s(\hat{\mathbf{r}},\xi_b))]. \quad (34)$$

It is easy to see from eqn (17) that the condition of locating the dividing surfaces becomes

$$\frac{\partial C_{\mathrm{dd}}(0;\xi_a,\xi_b)}{\partial \xi_a} = 0, \quad \frac{\partial C_{\mathrm{dd}}(0;\xi_a,\xi_b)}{\partial \xi_b} = 0. \quad (35)$$

In this case, locating the two optimized dividing surfaces is switched to finding the two optimized parameters (ξ_a,ξ_b).

4 Computational details

In the present study, the lattice model used consists of 817 Ni atoms and the Ni lattice constant is 3.52 Å. In the simulations, two hydrogen atoms (all six degrees of freedom) are treated quantum mechanically, while all the nickel atoms are rigid. In path integral calculations, the sampling of the discrete paths is performed using the Monte Carlo method. The number of time slices, P for the degrees of freedom of two H atoms, is set to P = (20–160) over the temperature range 160–800 K. The number of the Monte Carlo is about (4–8) $\times$ 10^6 for computing a single ensemble average. It converges most of the values within 10% statistical error.

5 Results and discussion

5.1 Free energy profile along the reaction path

We first calculate the free energy profile from the gas phase state (H_2(g) + S) to the chemisorbed state (2H(a) − S) at 300 K, with the two hydrogen atoms treated quantum mechanically. The results are displayed in Fig. 1. It is clearly shown that there is an obvious free energy well in the physisorbed state with a depth of 1.96 kcal mol^{-1} corresponding to the free energy in the gas phase state, and the dissociation and recombination free energy barriers for physisorbed H_2 are 2.82 and 17.46 kcal mol^{-1}, which demonstrate that the dissociation reaction of physisorbed H_2 is much easier than the recombination one. In Fig. 1, we also draw the geometries of H_2 in the gas phase state (GS, H_2 is located at about 6.0 bohr above the Ni(100) surface), the physisorbed state (PS, one H atom is located 2.07 bohr above a 4-fold site, and the other resides at 2.67 bohr near the neighboring bridge site), the transition state (TS, one H atom is located 1.12 bohr above a 4-fold site, and the other resides at 2.43 bohr near the neighboring bridge site) and the chemisorbed state (CS, both H atoms are adsorbed at 1.01 bohr above two nearest 4-fold sites) with 6 Ni atoms. It is noted that the distance of the center of mass of H_2 to the surface gradually

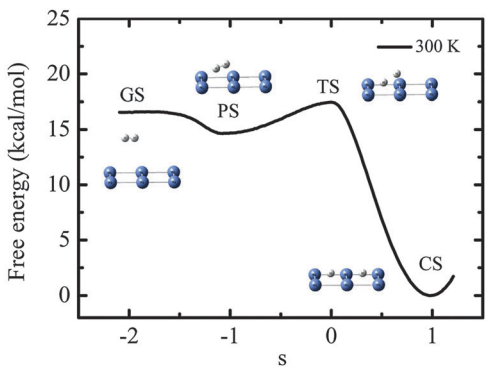

Fig. 1 Free energy profile along the reaction path for H_2/Ni(100) at 300 K. 'GS', 'PS', 'TS' and 'CS' stand for the gas phase, physisorbed, transition and chemisorbed states of H_2, respectively.

decreases, while the distance of two H atoms increases monotonically, from GS, PS, TS, to CS.

5.2 Dissociation and recombination rates of physisorbed H_2

Based on the free energy profile, we can calculate the dissociation (H_2(a) − S → 2H(a) − S) and recombination (2H(a) − S → H_2(a) − S) rates of physisorbed H_2 on the rigid Ni(100) surface, which correspond to k_2 and k_{-2} (eqn (2)), respectively. In order to investigate the quantum effect of H_2 motions on the rates, we also calculate the corresponding classical rates, labeled as QI_{cl}, with use of the classical limit of QI. The previous studies[66,81] have demonstrated that the classical limit of the QI formula is the same as the rate constant expression of the classical transition state theory (TST). Essentially, the time slice $P \to 1$ in the path integral corresponds to the classical limit of QI. However, according to eqn (21), P must be even and the minimum P is 4. Thus, $P = 4$ is used in the present work. These classical QI rates should have the similar property as the classical TST rates although they are not exactly the same. In Table 1, we summarize the present QI and QI_{cl} rates for both k_2 and k_{-2}, as well as the results of canonical variational transition state theory with the small-curvature semiclassical adiabatic approximation (CVT/SCSAG).[26] We also tabulate the ratios of quantum and classical rates in Table 1.

Fig. 2 displays the corresponding Arrhenius plots of rates. For the values of k_2, the QI and QI_{cl} have an obvious difference over the whole tested temperature range. At 800 K, the QI is 1.21 times larger than the QI_{cl}, considering that our classical simulation ($P = 4$) can be enough to capture most of zero point energy at 800 K, it is clear that the difference between QI and QI_{cl} should mainly come from the tunneling effect, which usually enhances the rate by lowering the free energy barrier. Indeed, the classical free energy barrier is higher than the quantum one by 0.2 kcal mol^{-1} at 800 K. At 200 K, the ratio of QI and QI_{cl} increases to 42.9, this remarkable difference is due to both the zero point energy and tunneling effect, indeed, the zero point energy correction can decrease the effective potential barrier by 0.8 kcal mol^{-1}, and our calculated classical free energy barrier is 1.0 kcal mol^{-1} higher than the quantum one. All these situations reveal that the quantum effect of H_2 is remarkable at both low and high temperatures for this process.

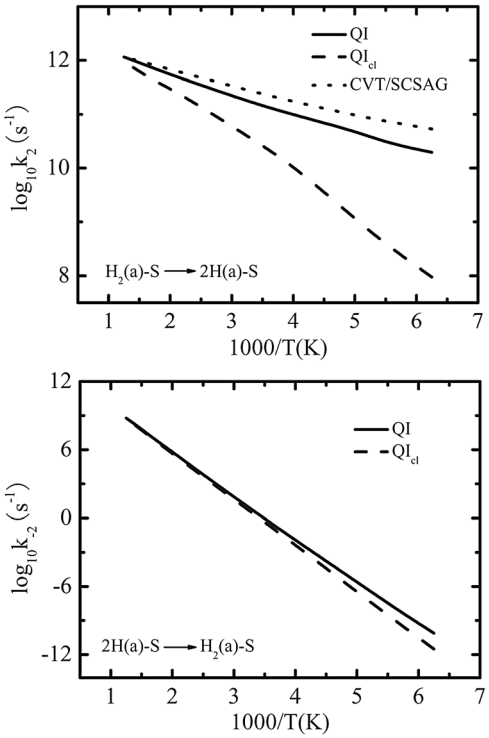

Fig. 2 Arrhenius plots of dissociation and recombination rate constants for physisorbed H_2 on a Ni(100) surface. The solid and dashed lines are the QI results with H atoms treated quantum mechanically and classically, respectively, and the dotted line denotes the rates of CVT/SCSAG.

Table 1 Rate constants[a] of the physisorbed H_2 on the Ni(100) surface

	k_2				k_{-2}		
T (K)	CVT/SCSAG[b]	QI	QI_{cl}[c]	QI/QI_{cl}	QI	QI_{cl}	QI/QI_{cl}
160	5.36(10)	1.97(10)	9.50(7)	207	7.68(−11)	3.14(−12)	24.4
180	7.28(10)	2.88(10)	3.52(8)	81.7	2.12(−8)	1.83(−9)	11.6
200	9.63(10)	4.91(10)	1.14(9)	42.9	2.54(−6)	3.39(−7)	7.51
250	1.72(11)	9.83(10)	1.12(10)	8.80	1.16(−2)	4.50(−3)	2.58
300	2.67(11)	1.65(11)	3.47(10)	4.75	3.75(0)	2.08(0)	1.80
400	4.78(11)	3.49(11)	1.39(11)	2.52	6.25(3)	4.26(3)	1.47
500	6.82(11)	5.49(11)	3.00(11)	1.83	6.56(5)	4.63(5)	1.42
600	8.63(11)	7.67(11)	4.66(11)	1.64	1.27(7)	1.06(7)	1.20
800	1.16(12)	1.15(12)	9.53(11)	1.21	6.01(8)	5.56(8)	1.08

[a] Unit: s^{-1}, powers of 10 are in parentheses. [b] From ref. 26. [c] QI_{cl} denotes the classical limit of QI rates.

Based on the same PES adopted in the present work, Truong *et al.*[26] have applied the steady state approximation which assumes that the physisorbed H_2 is in equilibrium, and reported the rates (k_2) using canonical variational transition state theory with semiclassical tunneling approximation (CVT/SCSAG). Comparing the QI rates with that of CVT/SCSAG, as shown in Fig. 2, we can see they are in good agreement with each other at high temperatures, however, the QI is smaller than the CVT/SCSAG at low temperatures even though they still have the same orders of magnitude, this discrepancy is mainly caused by the fact that these two methods have used different ways to incorporate the tunneling effect, and the tunneling effect affects the rates a lot at low temperatures.

Chakravarty and Metiu[59] have reported a value of 1.9×10^8 (s^{-1}) for k_2 at 300 K, which is much lower than that of the QI and the CVT/SCSAG, the main reason is that Chakravarty and Metiu's method does not consider the quantum effect (such as zero point energy correction and quantum tunneling), indeed, the zero point energy correction can decrease the effective potential barrier by 0.8 kcal mol^{-1}. Another reason is that Chakravarty and Metiu's method has incorporated the recrossing effect, which usually decreases the rates, while the QI and CVT theories do not take it into account, this situation reflects that the recrossing effect may also be remarkable for the present process.

For the recombination process (k_{-2}), Fig. 2 shows that QI and QI_{cl} are close to each other at high temperatures, while the classical rates become much smaller than the quantum ones at low temperatures. At 800 K, the QI is 1.08 times larger than the QI_{cl}, and the rate ratio increases to 7.51 at 200 K. These phenomena can also be explained by the differences in quantum and classical free energy barriers, indeed, the calculated quantum and classical free energy barriers are nearly the same at 800 K and the former is about 0.5 kcal mol^{-1} lower than the latter at 200 K. Experimentally, Zhu and White[8] have reported an activation energy of 22.7($\pm$0.2) kcal mol^{-1} and a preexponential factor of 1.5 $\pm$ 0.6($\times 10^{14}$) ML^{-1} s^{-1} in the temperature range of 300–340 K. To compare with it, we calculate the activation energy (E_a) and preexponential factor (A) by fitting the QI rates to the Arrhenius form

$$k_{QI} = A \exp[-E_a/RT] \quad (36)$$

over the temperature range 250–400 K. The calculated E_a and A are 17.48 kcal mol^{-1} and 2.23 $\times$ 10^{13} s^{-1}, it is clear that our preexponential is consistent with the experimental data but the activation energy is much smaller. This much smaller activation energy reveals that the recombination potential barrier of the present PES may need to be further refined.

5.3 Kinetic isotope effects for physisorbed H_2

The kinetic isotope effect (KIE) is defined as the ratio k^i/k^j, where k^i is the rate for the isotopic reaction with lighter mass, and k^j is that for the corresponding heavier isotopic reaction. Here, we consider the KIEs of the dissociation (k_2) and recombination (k_{-2}) processes by examining the values of $k_2(H_2)/k_2(D_2)$ and $k_{-2}(H_2)/k_{-2}(D_2)$. These KIE values are tabulated in Table 2, in which we also list the CVT/SCSAG results.[26]

From Table 2, we can know that the dissociation rates (k_2) of physisorbed H_2 and D_2 are in the same orders of magnitude, and the rates of H_2 are larger than that of D_2. The recombination rates (k_{-2}) of H_2 and D_2 have the same trend as that of the dissociation ones. These differences between the rates of H_2 and D_2 can be explained by the differences in free energy profiles. Fig. 3 displays the dissociation and recombination free energy profiles for physisorbed H_2 and D_2 at 300 K. Explicitly, both the dissociation and recombination free energy barriers of physisorbed H_2 are lower than that of D_2 by 0.26 and 0.44 kcal mol^{-1} at 300 K.

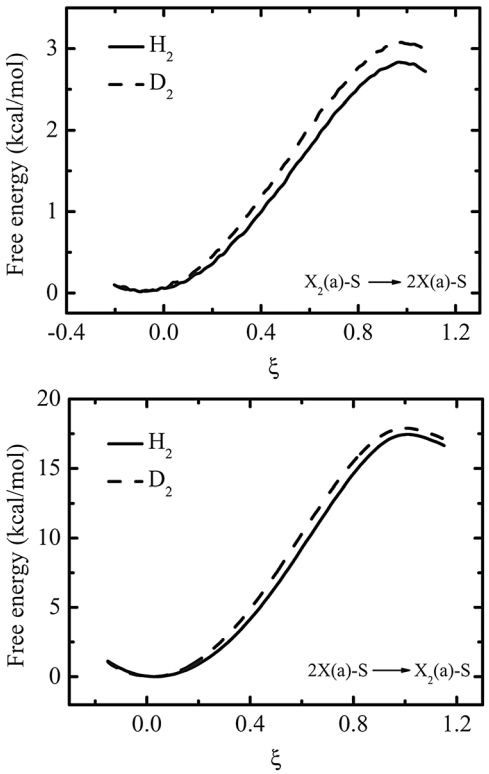

Fig. 3 Free energy profiles of dissociation and recombination for two isotopic reactions at 300 K. The solid and dashed lines are the results corresponding to H_2 and D_2, respectively.

Table 2 The kinetic isotope effects (KIEs) of physisorbed H_2

	KIE(k_2)		KIE(k_{-2})
T (K)	QI(H_2/D_2)	CVT/SCSAG(H_2/D_2)[a]	QI(H_2/D_2)
160	4.02	6.37	12.1
180	3.33	5.09	9.25
200	3.18	4.32	6.20
250	2.50	3.26	3.31
300	2.18	2.79	2.27
400	2.11	2.34	2.09
500	2.10	2.12	1.93
600	2.12	1.97	1.66
800	1.85	1.79	1.55

[a] From ref. 26.

Table 2 shows that the KIEs are remarkable for both processes. The values of $k_2(H_2)/k_2(D_2)$ are 4.02, 3.18, 2.18, 2.10 and 1.85, and the values of $k_{-2}(H_2)/k_{-2}(D_2)$ are 12.1, 6.20, 2.27, 1.93 and 1.55 at 160, 200, 300, 500 and 800 K, respectively. Both KIEs increase with decreasing temperature, this behavior is due to the fact that the tunneling effect enhances the rates of H_2 much larger than that of D_2 at low temperatures.

Comparing the values of QI(H_2/D_2) with the results of CVT/SCSAG, we can see that they are in good agreement with each other at high temperatures, however, the QI ones are smaller than that of CVT/SCSAG at low temperatures. These discrepancies at low temperatures can be explained by the fact that the QI and CVT/SCSAG have used different ways to incorporate the tunneling effect and the tunneling effect affects the KIE a lot.

5.4 The total rates of H_2 on the Ni(100)

In the above sections, we have calculated the dissociation rates (k_2) of physisorbed H_2 on the rigid Ni(100) surface, considering that the k_1 and k_{-1} should not be affected by the tunneling effect, we use the CVT data[26] of k_1 and k_{-1} directly in our following calculations. With use of these rates, we can obtain the steady state rate k_{steady} (as seen in eqn (3)) under steady state approximation. We can also calculate the direct rate (k_{direct}) using a direct reaction mechanism by ignoring the physisorbed state. The total rate (k) is a combination of the k_{steady} and k_{direct} as shown in eqn (10).

Table 3 Rate constants[a] for H_2 on the Ni(100) surface

T (K)	k_1[b]	k_{-1}[b]	k_2[c]	k_{steady}	k_{direct}	f_{MB}	k
160	4.43(−11)	8.20(11)	1.97(10)	1.04(−12)	4.50(−12)	3.72(−6)	1.04(−12)
180	2.28(−11)	1.03(12)	2.88(10)	6.19(−13)	4.31(−12)	1.84(−5)	6.19(−13)
200	2.56(−11)	1.42(12)	4.91(10)	8.55(−13)	3.26(−12)	6.55(−5)	8.55(−13)
250	1.91(−11)	2.61(12)	9.83(10)	6.93(−13)	2.32(−12)	6.62(−4)	6.94(−13)
300	7.72(−12)	3.70(12)	1.65(11)	3.29(−13)	1.90(−12)	3.00(−3)	3.34(−13)
400	4.17(−12)	4.88(12)	3.49(11)	2.78(−13)	1.68(−12)	1.90(−2)	3.05(−13)
500	3.09(−12)	5.82(12)	5.49(11)	2.66(−13)	1.73(−12)	5.61(−2)	3.49(−13)
600	2.68(−12)	6.56(12)	7.67(11)	2.81(−13)	1.87(−12)	1.13(−1)	4.60(−13)
800	1.49(−12)	4.51(12)	1.15(12)	3.03(−13)	2.38(−12)	2.64(−1)	8.51(−13)

[a] Unit: cm^3 $site^{-1}$ s^{-1} for k_1, k_{steady}, k_{direct} and k; s^{-1} for k_{-1} and k_2; powers of 10 are in parentheses. [b] k_1 and k_{-1} are the CVT results from ref. 26. [c] k_2 is the QI rates.

Table 3 lists the k_1, k_{-1}, k_2, k_{steady}, k_{direct}, f_{MB} and k for H_2 at temperatures ranging from 160–800 K, the corresponding Arrhenius plots are displayed in Fig. 4. For the H_2 dissociation, both the k_{steady} and k_{direct} have nonmonotonic behaviors with larger values at both low and high temperatures. The increase of k_{direct} at high temperatures is due to the fact that it is an activated process, while the increase of k_{direct} at low temperatures is most probably caused by the quantum effect, as seen in Fig. 5, the effective free energy barriers from the gas phase to the transition state become very low at low temperatures. The direct process seems like a non-activated process at very low temperatures, under this situation, the steering effect may play an important role.

We can also see that the k_{direct} is always much larger than k_{steady}, and the ratio of k_{direct} and k_{steady} is 5.78 at 300 K, this discrepancy is caused by the fact that the zero point energy corrected potential barrier for the direct process is only 0.6 kcal mol^{-1}, which is much lower than the effective potential barrier (2.0 kcal mol^{-1}) of physisorbed H_2.

In order to obtain the total rate k, we calculate the fraction (f_{MB}) of gas phase hydrogen molecules with translational energy equal to or in excess of a certain energy ($4.75(\text{kcal mol}^{-1}) - k_BT$) with the Maxwell–Boltzmann distribution. In Table 3, we can see that the values of f_{MB} are very small at low temperatures, which means only the steady state process is allowed for the H_2, and the f_{MB} increases with increasing temperature, which demonstrates that more and more hydrogen molecules are undergo a direct process of dissociation. However, even at 800 K, only 26% of gas phase H_2 are able to dissociate directly. With use of the f_{MB}, the total rate k is calculated. In Fig. 4, we can see the total rate k has the form of an inverted bell, and its minimum value appears at about 400 K, at which the contributions of k_{steady} and k_{direct} to k are 89% and 11%, respectively. At low temperatures, k is equal to k_{steady} because the f_{MB} is very close to zero, while it becomes close to k_{direct} at high temperatures with the increase of f_{MB}, for instance, the contributions of k_{steady} and k_{direct} to k are 26% and 74% at 800 K. We have plotted the free energy profiles from the gas phase to the transition state at different temperatures in Fig. 5. It is clear that the free energy well at the physisorbed state is very deep at low temperatures, however, it becomes shallow with the increase of temperature, which demonstrates that the hydrogen molecules become less favorable to reside at the physisorption site at high temperatures. Finally, we can conclude that the dissociation of H_2 mainly proceeds through a physisorbed state below 400 K, but both the direct and physisorbed dynamics are important above 400 K.

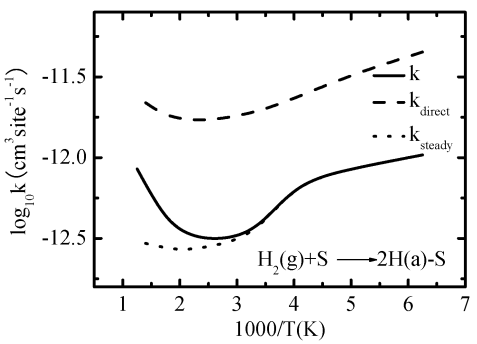

Fig. 4 Arrhenius plots of rate constants for H_2 on Ni(100). The solid, dashed and dotted lines are the total rate k, k_{direct} and k_{steady}, respectively.

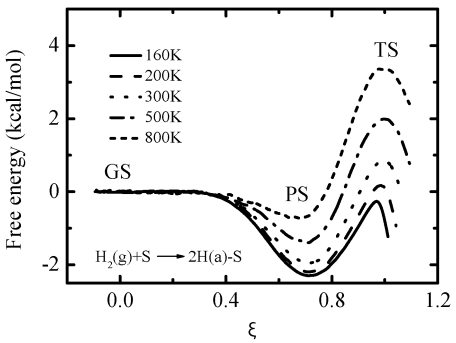

Fig. 5 Free energy profiles from the gas phase state to the transition state for H_2 on Ni(100). The solid, dashed, dotted, dash-dotted and short dashed lines are the results corresponding to 160, 200, 300, 500 and 800 K, respectively.

Compared with others, Chakravarty and Metiu[59] used the classical correlation function theory and reported that H_2 is first physisorbed and then dissociated at 100 K, which is in good agreement with our conclusion at low temperatures, however, they treated the dynamics as a direct dissociation and ignored physisorption at 300 K, which conflicts with ours that the physisorbed dynamics still play an important role even above 300 K.

Table 4 Rate constants[a] for D_2 on the Ni(100) surface

T (K)	k_1[b]	k_{-1}[b]	k_2[c]	k_{steady}	k_{direct}	f_{MB}	k
160	1.63(−11)	3.22(11)	4.90(9)	2.44(−13)	1.09(−12)	1.64(−5)	2.44(−13)
180	1.10(−11)	5.16(11)	8.64(9)	1.81(−13)	8.23(−13)	6.81(−5)	1.81(−13)
200	8.07(−12)	7.59(11)	1.54(10)	1.61(−13)	7.06(−13)	2.22(−4)	1.61(−13)
250	4.79(−12)	1.54(12)	3.94(10)	1.19(−13)	6.71(−13)	1.69(−3)	1.20(−13)
300	3.50(−12)	2.47(12)	7.57(10)	1.04(−13)	6.05(−13)	6.44(−3)	1.07(−13)
400	2.61(−12)	4.53(12)	1.65(11)	9.18(−14)	6.11(−13)	3.32(−2)	1.09(−13)
500	1.22(−12)	3.34(12)	2.61(11)	8.85(−14)	6.80(−13)	8.69(−2)	1.40(−13)
600	8.99(−13)	3.08(12)	3.63(11)	9.47(−14)	8.76(−13)	1.62(−1)	2.21(−13)
800	6.61(−13)	2.63(12)	6.23(11)	1.27(−13)	1.18(−12)	3.39(−1)	4.83(−13)

[a] Unit: $cm^3\ site^{-1}\ s^{-1}$ for k_1, k_{steady}, k_{direct} and k; s^{-1} for k_{-1} and k_2; powers of 10 are in parentheses. [b] k_1 and k_{-1} are the CVT results from ref. 26. [c] k_2 is the QI rates.

5.5 The total rates of D_2 on the Ni(100)

We also calculate the k_{steady} and k_{direct} for D_2 on the Ni(100) surface, as well as the fraction (f_{MB}) of D_2 with translational energy equal to or in excess of a certain energy ($4.26(kcal\ mol^{-1}) - k_BT$). All the values are tabulated in Table 4, and the corresponding Arrhenius plots are displayed in Fig. 6.

In Table 4, we can see the k_{direct} is always much larger than k_{steady} over the whole tested temperature range 160–800 K, for instance, the ratio of k_{direct} and k_{steady} is 5.82 at 300 K, this phenomenon is because the effective potential barriers for the direct dynamics and physisorbed D_2 are 0.36 and 2.26 kcal mol^{-1}, respectively. Fig. 6 shows that both k_{direct} and k_{steady} decrease firstly, then they reach minimum values at about 300 and 500 K, respectively, finally they increase with increasing temperature. The total rate k is calculated with k_{direct} and k_{steady} according to eqn (10), it is noted that the total rate k is exactly the same as k_{steady} at low temperatures, while it gets close to k_{direct} with the increase of temperature. The total rate k of D_2 also has the form of an inverted bell, with a minimum at about 300 K, below which the steady state dynamics dominates the dissociation process.

5.6 Kinetic isotope effects for the total rate

The kinetic isotope effects of H_2/D_2 for k_{steady}, k_{direct} and k are calculated and tabulated in Table 5, in this table we also include the CVT/SCSAG results[26] under steady state approximation. We can see that all the KIEs are much larger than 1, this situation reveals that the rates of H_2 are always larger than that of D_2, which qualitatively agrees with the experimental data[5] that the D_2 has a larger dissociation barrier. It is interesting to notice that the KIEs of k_{steady}, k_{direct} and k are all nonmonotonic with respect to temperature, they first increase to maxima, then decrease, and the maximum values are 5.81, 4.63 and 5.77 at 250, 200 and 250 K, respectively. The values in Table 5 also show that the KIEs of k_{steady} are larger than that of k_{direct} over the whole tested temperature range. The KIEs of k are close to that of k_{steady} at low temperatures, while they become smaller than both k_{steady} and k_{direct} at high temperatures.

Table 5 The kinetic isotope effects for the total reaction

	KIEs(H_2/D_2)			
T (K)	k_{steady}	k_{steady}(CVT/SCSAG)[a]	k_{direct}	k
160	4.25	6.6	4.13	4.25
200	5.32	6.6	4.63	5.32
250	5.81	4.5	3.46	5.77
300	3.17	4.0	3.14	3.11
400	3.03	3.3	2.76	2.79
500	3.01	3.0	2.55	2.49
600	2.96	2.8	2.14	2.08
800	2.39	2.3	2.02	1.76

[a] From ref. 26.

Comparing our QI KIEs of k_{steady} to that of CVT/SCSAG, we find that the QI is in good agreement with CVT/SCSAG at high temperatures, however, it is smaller at low temperatures. Truong *et al.* have attributed the large KIEs at low temperatures to the tunneling effect, so the difference between the QI and CVT/SCSAG is mainly caused by the fact that these two methods have used different ways to incorporate the tunneling effect.

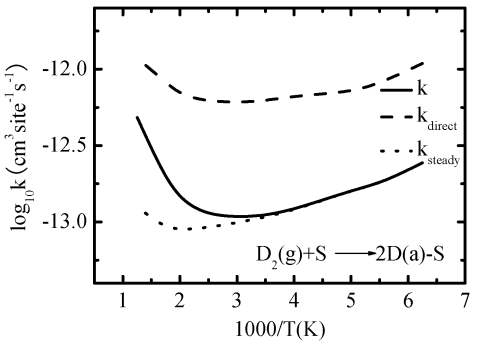

Fig. 6 Arrhenius plots of rate constants for D_2 on Ni(100). The solid, dashed and dotted lines are the total rate k, k_{direct} and k_{steady}, respectively.

6 Concluding remarks

We have calculated the dissociation and recombination rates of physisorbed H_2, the total dissociation rate of gas phase H_2, and the corresponding kinetic isotope effects on the rigid Ni(100) surface, using the quantum instanton approximation with the modified version of Lee and DePristo's potential energy surface.

For the dissociation and recombination reactions of physisorbed H_2, we have calculated the quantum and classical rates by considering H atoms as quantum and classical particles, respectively. Both the dissociation and recombination rates show that the quantum rates are obviously larger than the classical

ones, especially at low temperatures. This behavior has been explained by the quantum effect that lowers the free energy barriers and enhances the rates. Our fitted activation energy (17.48 kcal mol^{-1}) for the recombination process is much lower than the experimental one (22.7 kcal mol^{-1}), this shows that the recombination barrier of the present PES should be refined. The obtained kinetic isotope effects of H_2/D_2 are consistent with that of CVT/SCSAG, and the increase of the KIEs with decreasing temperature demonstrates that the tunneling effect is remarkable.

We have also calculated the steady state, direct and total dissociation rates of gas phase H_2 on the Ni(100) surface, and found that the steady state and direct dissociation rates have minimum values at about 400–500 K, while the total one has the form of inverted bell with respect to temperature. We also demonstrate that, under the conditions that the physisorbed state exists, the gas phase H_2 has two ways to dissociate, one is the steady state process that physisorbed H_2 is formed, equilibrated and dissociated, the other is the direct process that H_2 passes over the physisorbed state directly. Detailed analysis shows that the dissociation of gas phase H_2 is dominated by the steady state process below 400 K, however, both the steady state and direct processes are important above 400 K. The calculated KIEs for the rates reveal that H_2 always has larger rates than D_2 no matter which dissociation process they undergo, and the direct process has a smaller KIE than the steady state process.

Appendix: the analytical result of $C_{dd}(0)/Q_r$

We now consider how to obtain $C_{dd}(0)/Q_r$ analytically for the direct process (eqn (4)). For the rigid surface, the Hamiltonian of the system can be written as

$$\hat{H} = \frac{\hat{P}_R^2}{2m_c} + \frac{\hat{P}_r^2}{2\mu_r} + V(\hat{R}, \hat{r}), \tag{A.1}$$

where the scattering vector R connects the Ni(100) surface and the center of mass of H_2, the interatomic vector r connects two hydrogen atoms, P_R and P_r are the momenta conjugate to R and r, respectively, while the m_c and μ_r are the mass of the center of mass and the reduced mass of H_2, respectively.

In the gas phase state, H_2 is far away from the Ni(100) surface, and the interaction potential energy between H_2 and the surface is negligible, so the Hamiltonian can be further written as

$$\hat{H} \approx \frac{\hat{P}_R^2}{2m_c} + \frac{\hat{P}_r^2}{2\mu_r} + V(\hat{r}) \;=\; \hat{H}_R + \hat{H}_r. \tag{A.2}$$

The term $C_{dd}(0)/Q_r$ has the form that

$$\begin{aligned} C_{dd}(0)/Q_r \;=& \frac{\mathrm{tr}\left[e^{-\beta\hat{H}/2}\Delta(s_a)e^{-\beta\hat{H}/2}\Delta(s_b)\right]}{\mathrm{tr}\left[e^{-\beta\hat{H}/2}\delta(s_a^0)e^{-\beta\hat{H}/2}\delta(s_b^0)\right]} \\ &\times \frac{\mathrm{tr}\left[e^{-\beta\hat{H}/2}\delta(s_a^0)e^{-\beta\hat{H}/2}\delta(s_b^0)\right]}{Q_r}, \end{aligned} \tag{A.3}$$

where the first term on the right has been discussed in Section 3.2, and the second term can be evaluated analytically. Following the previous studies,[66,81] and considering that s_a^0 and s_b^0 are only related to the scattering vector R in the gas phase state, we can get

$$\begin{aligned} &\mathrm{tr}\left[e^{-\beta\hat{H}/2}\delta(s_a^0)e^{-\beta\hat{H}/2}\delta(s_b^0)\right] \\ &= \mathrm{tr}\left[e^{-\beta\hat{H}_r}\right] \times \mathrm{tr}\left[e^{-\beta\hat{H}_R/2}\delta(s_a^0)e^{-\beta\hat{H}_R/2}\delta(s_b^0)\right] \\ &= \mathrm{tr}\left[e^{-\beta\hat{H}_r}\right] \times 2\left(\frac{m_c}{2\pi\hbar^2\beta}\right)^2, \end{aligned} \tag{A.4}$$

and

$$\begin{aligned} Q_r \;&= \mathrm{tr}\left[e^{-\beta\hat{H}_r}\right] \times \mathrm{tr}\left[e^{-\beta\hat{H}_R}\right] \\ &= \mathrm{tr}\left[e^{-\beta\hat{H}_r}\right] \times \left(\frac{m_c}{2\pi\hbar^2\beta}\right)^{3/2}. \end{aligned} \tag{A.5}$$

Finally, we obtain

$$\frac{\mathrm{tr}\left[e^{-\beta\hat{H}/2}\delta(s_a^0)e^{-\beta\hat{H}/2}\delta(s_b^0)\right]}{Q_r} = \left(\frac{2m_c}{\pi\hbar^2\beta}\right)^{1/2}. \tag{A.6}$$

Acknowledgements

This work was supported by the National Natural Science Foundation of China (Grant No. 21143007 and 21203151), National Basic Research Program of China (973 Program) (2013CB834602) and the Foundation of the State Key Laboratory for Physical Chemistry of Solid Surfaces, Xiamen University (No. 201116). The computational resources utilized in this research were provided by Shanghai Supercomputer Center.

References

1 G.-J. Kroes, *Prog. Surf. Sci.*, 1999, **60**, 1.
2 M. Bonn, A. M. Kleyn and G. J. Kroes, *Surf. Sci.*, 2002, **500**, 475.
3 G. Lanzani, R. Martinazzo, G. Materzanini, I. Pino and G. F. Tantardini, *Theor. Chem. Acc.*, 2007, **117**, 805.
4 D. Farias and R. Miranda, *Prog. Surf. Sci.*, 2011, **86**, 222.
5 A. V. Hamza and R. J. Madix, *J. Phys. Chem.*, 1985, **89**, 5381.
6 S. Andersson, *Chem. Phys. Lett.*, 1978, **55**, 185.
7 X. Y. Zhu, S. Akhter, M. E. Castro and J. M. White, *Surf. Sci.*, 1988, **195**, L145.
8 X. Y. Zhu and J. M. White, *J. Phys. Chem.*, 1988, **92**, 3970.
9 H. P. Steinruck, M. Luger, A. Winkler and K. D. Rendulic, *Phys. Rev. B: Condens. Matter Mater. Phys.*, 1985, **32**, 5032.
10 K. D. Rendulic, G. Anger and A. Winkler, *Surf. Sci.*, 1989, **208**, 404.
11 X. Y. Zhu, M. E. Castro and J. M. Whilte, *J. Chem. Phys.*, 1989, **90**, 7442.
12 A. E. Baber, H. L. Tierney, T. J. Lawton and E. C. H. Sykes, *ChemCatChem*, 2011, **3**, 607.
13 J. K. Norskov, *J. Chem. Phys.*, 1989, **90**, 7461.
14 C. Lee and A. E. DePristo, *J. Chem. Phys.*, 1986, **84**, 485.
15 C.-Y. Lee and A. E. DePristo, *J. Chem. Phys.*, 1986, **85**, 4161.

16 J. Mei, J. W. Davenport and G. W. Fernando, *Phys. Rev. B: Condens. Matter Mater. Phys.*, 1991, **43**, 4653.
17 T. N. Truong, D. G. Truhlar and B. C. Garrett, *J. Phys. Chem.*, 1989, **93**, 8227.
18 T. N. Truong and D. G. Truhlar, *J. Phys. Chem.*, 1990, **94**, 8262.
19 G. Kresse, *Phys. Rev. B: Condens. Matter Mater. Phys.*, 2000, **62**, 8295.
20 A. Gruneich, A. J. Cruz and B. Jackson, *J. Chem. Phys.*, 1993, **98**, 5800.
21 A. J. Cruz and B. Jackson, *J. Chem. Phys.*, 1991, **94**, 5715.
22 B. Jackson and H. Metiu, *J. Chem. Phys.*, 1987, **86**, 1026.
23 J. Sheng and J. Z. H. Zhang, *J. Chem. Phys.*, 1992, **96**, 3866.
24 M.-N. Carre, B. Jackson and D. Lemoine, *J. Chem. Soc., Faraday Trans.*, 1997, **93**, 949.
25 C. Engdahl, B. I. Lundqvist, U. Nielsen and J. K. Norskov, *Phys. Rev. B: Condens. Matter Mater. Phys.*, 1992, **45**, 11362.
26 T. N. Truong, G. Hancock and D. G. Truhlar, *Surf. Sci.*, 1989, **214**, 523.
27 T. Panczyk, P. Szabelski and W. Rudzinski, *J. Phys. Chem. B*, 2005, **109**, 10986.
28 R. V. Harrevelt, K. Honkala, J. K. Norskov and U. Manthe, *J. Chem. Phys.*, 2005, **122**, 234702.
29 J.-C. Chen, J. C. Juanes-Marcos, S. Woittequand, M. F. Somers, C. Diaz, R. A. Olsen and G.-J. Kroes, *J. Chem. Phys.*, 2011, **134**, 114708.
30 T. J. Frankcombe and M. A. Collins, *Phys. Chem. Chem. Phys.*, 2011, **13**, 8379.
31 A. A. B. Padama, H. Kasai and H. Kawai, *Surf. Sci.*, 2012, **606**, 62.
32 K. Lee, K. Berland, M. Yoon, S. Andersson, E. Schroder, P. Hyldgaard and B. I. Lundqvist, *J. Phys.: Condens. Matter*, 2012, **24**, 424213.
33 J.-C. Chen, M. Ramos, C. Arasa, J. C. Juanes-Marcos, M. F. Somers, A. E. Martinez, C. Diaz, R. A. Olsen and G.-J. Kroes, *Phys. Chem. Chem. Phys.*, 2012, **14**, 3234.
34 S. Klacar and H. Gronbeck, *Catal. Sci. Technol.*, 2013, **3**, 183.
35 G. Fuchsel, J. C. Tremblay, T. Klamroth, P. Saalfrank and C. Frischkorn, *Phys. Rev. Lett.*, 2012, **109**, 098303.
36 G. Fuchsel, J. C. Tremblay, T. Klamroth and P. Saalfrank, *ChemPhysChem*, 2013, **14**, 1471.
37 G. Fuchsel, S. Schimka and P. Saalfrank, *J. Phys. Chem. A*, 2013, **117**, 8761.
38 P. S. Thomas, M. F. Somers, A. W. Hoekstra and G.-J. Kroes, *Phys. Chem. Chem. Phys.*, 2012, **14**, 8628.
39 A. Mondal, M. Wijzenbroek, M. Bonfanti, C. Diaz and G.-J. Kroes, *J. Phys. Chem. A*, 2013, **117**, 8770.
40 T. Liu, B. Fu and D. H. Zhang, *J. Chem. Phys.*, 2013, **139**, 184705.
41 B. Jiang, R. Liu, J. Li, D. Xie, M. Yang and H. Guo, *Chem. Sci.*, 2013, **4**, 3249.
42 S. B. Donald, J. K. Navin and I. Harrison, *J. Chem. Phys.*, 2013, **139**, 214707.
43 T. Liao, C. Sun, Z. Sun, A. Du and S. Smith, *Phys. Chem. Chem. Phys.*, 2013, **15**, 8054.
44 S. B. Donald and I. Harrison, *J. Phys. Chem. C*, 2014, **118**, 320.
45 M. Wijzenbroek and G. J. Kroes, *J. Chem. Phys.*, 2014, **140**, 084702.
46 M. Hand and J. Harris, *J. Chem. Phys.*, 1990, **92**, 7610.
47 M. Dohle and P. Saalfrank, *Surf. Sci.*, 1997, **373**, 95.
48 A. K. Tiwari, S. Nave and B. Jackson, *J. Chem. Phys.*, 2010, **132**, 134702.
49 M. Bonfanti, C. Diaz, M. F. Somers and G.-J. Kroes, *Phys. Chem. Chem. Phys.*, 2011, **13**, 4552.
50 T. Sahoo, S. Sardar, P. Mondal, B. Sarkar and S. Adhikari, *J. Phys. Chem. A*, 2011, **115**, 5256.
51 T. Sahoo, S. Sardar and S. Adhikari, *Phys. Chem. Chem. Phys.*, 2011, **13**, 10100.
52 Y. V. Suleimanov, *J. Phys. Chem. C*, 2012, **116**, 11141.
53 W. Wang and Y. Zhao, *J. Phys. Chem. C*, 2013, **117**, 19010.
54 A. Gross, S. Wilke and M. Scheffler, *Phys. Rev. Lett.*, 1995, **75**, 2718.
55 A. Gross and M. Scheffler, *Phys. Rev. B: Condens. Matter Mater. Phys.*, 1998, **57**, 2493.
56 P. A. Karlsson, A. S. Martensson and S. Andersson, *Surf. Sci.*, 1986, **175**, L759.
57 L. Westerlund, L. Jonsson and S. Andersson, *Surf. Sci.*, 1988, **199**, 109.
58 M. A. D. Cesare, H. F. Busnengo, W. Dong and A. Salin, *J. Chem. Phys.*, 2003, **118**, 11226.
59 C. Chakravarty and H. Metiu, *J. Chem. Phys.*, 1995, **102**, 8643.
60 R. C. Mowrey, *J. Chem. Phys.*, 1993, **99**, 7049.
61 W. H. Miller, Y. Zhao, M. Ceotto and S. Yang, *J. Chem. Phys.*, 2003, **119**, 1329.
62 W. H. Miller, *J. Chem. Phys.*, 1975, **62**, 1899.
63 S. Coleman, *Phys. Rev. D: Part. Fields*, 1977, **15**, 2929.
64 T. Yamamoto and W. H. Miller, *J. Chem. Phys.*, 2004, **120**, 3086.
65 Y. Zhao, T. Yamamoto and W. H. Miller, *J. Chem. Phys.*, 2004, **120**, 3100.
66 W. Wang, S. Feng and Y. Zhao, *J. Chem. Phys.*, 2007, **126**, 114307.
67 M. Buchowiecki, *Chem. Phys. Lett.*, 2012, **531**, 202.
68 T. Yamamoto and W. H. Miller, *J. Chem. Phys.*, 2005, **122**, 044106.
69 K. F. Wong, J. L. Sonnenberg, F. Paesani, T. Yamamoto, J. Vanicek, W. Zhang, H. B. Schlegel, D. A. Case, T. E. Cheatham III, W. H. Miller and G. A. Voth, *J. Chem. Theory Comput.*, 2010, **6**, 2566.
70 W. Wang and Y. Zhao, *J. Chem. Phys.*, 2009, **130**, 114708.
71 W. Wang and Y. Zhao, *J. Chem. Phys.*, 2010, **132**, 064502.
72 Y. Zhao and W. Wang, *Adv. Phys. Chem.*, 2012, **2012**, 483504.
73 W. Wang and Y. Zhao, *Phys. Chem. Chem. Phys.*, 2011, **13**, 19362.
74 W. Wang and Y. Zhao, *J. Chem. Phys.*, 2012, **137**, 214306.
75 J. Vanicek, W. H. Miller, J. F. Castillo and F. J. Aoiz, *J. Chem. Phys.*, 2005, **123**, 054108.
76 J. Vanicek and W. H. Miller, *J. Chem. Phys.*, 2007, **127**, 114309.
77 T. Zimmermann and J. Vanicek, *J. Chem. Phys.*, 2009, **131**, 024111.
78 J. Huang, M. Buchowiecki, T. Nagy, J. Vanicek and M. Meuwly, *Phys. Chem. Chem. Phys.*, 2014, **16**, 204.
79 D. M. Ceperley, *Rev. Mod. Phys.*, 1995, **67**, 279.
80 C. Bartels and M. Karplus, *J. Comput. Chem.*, 1997, **18**, 1450.
81 C. Preduscu and W. H. Miller, *J. Phys. Chem. B*, 2005, **109**, 6491.

